8. SLOWING-DOWN IN NON-CIRCULAR TOKAMAKS

To fully describe the collisional slowing-down of fast ions in non-circular tokamaks, the formulation of Chapter 7 has been extended to include large banana-width effects.

8.1 Previous Work

Fast ion dynamics have been studied extensively in the small banana-width limit. In the so-called "retardation theory" [1,47, 52-56], energetic ions are viewed as test particles undergoing collisional relaxation in a uniform background plasma. Ion and electron heating rates are obtained from the "instantaneous heating" or "in-situ" deposition model (for example, see Refs. 57-58) by assuming that the energy relaxation time is nearly zero, and thus all the energy is deposited on the flux surface where the particle is born. Numerous workers [18,45,59-76] have calculated fast ion distributions using the small banana-width, bounce-averaged Fokker-Planck equation, including the effects of speed-diffusion, pitch-angle scattering, the velocity-space loss-region, toroidal electric field, impurities, charge exchange, and time delay in heating due to finite slowing down time. Trapped particle contributions have been examined analytically by Cordey [45] and via Monte Carlo calculations by Killeen et al [77] and Goldston [99], yielding inward (outward) slowing-down drifts (relative to the plasma center) for co-(counter) going ions. (The present work finds that these

results need clarification; see Chapter 11.) The additional effect of large energy transfer (LET) interactions has been modeled by the multi-group method [78-80] and by quantum mechanics, including nuclear and coulomb scattering plus spin [81]. However, for alpha particles, LET effects are small for $T_i \sim T_e \lesssim 20$ KeV, as inferred from Figs. 4-5 of Ref. 82. Still, the above models are inadequate for describing alpha particle effects because the small banana-width approximation is used.

More recently, the detailed properties of large banana-width orbits have been studied [4,13,16-17,35,54,117], and corresponding neoclassical transport models developed. The early attempts to model α heating used only the initial orbits ("single orbit" approximation), described as circles [15] and as finite width bananas [83]. Later, Petrie and Miley [8] calculated alpha power deposition using a spatial- and phase-group method to follow the evolving guiding-center orbits during the slowing-down process. In the light of the present work, the drifts obtained by Ref. 43 are consistent with Refs. 29-30 (see Ch. 11). Ohnishi et al. [35] examined alpha losses to the first wall during slowing down and pitch-angle scattering using a Monte Carlo Technique. Recently, Mikkelsen and Post [84] have developed a Monte Carlo alpha heating code, including first-orbit losses, finite slowing down time, and orbit drifts. Using these techniques, it is relatively easy to obtain moments of the disbribution function because integration

smooths out discrete particle effects, but large amounts of computer time (because of slow numerical convergence) are required to find the distribution function itself (for comparison with charge-exchange data). In all the studies cited here, anamolous slowing effects (e.g. Refs. 2 and 33) are ignored.

The present work is based on classical slowing down, which has been well tested by neutral injection experiments at energies, $E \lesssim 100$ keV. More recently, fusion-produced tritium ($E \lesssim 1$ MeV) experiments in PLT [100] have demonstrated thermalization consistent with the classical model. Since fast ion transport scales [4] like the (charge)/(momentum), the 1-MeV T results apply to 3.5-MeV alphas as well (c.f. eqn. 2.9).

The present method consists of bounce-averaging the Fokker-Planck equation after the variables have been transformed to the three constants-of-motion (COM) which characterize the orbit of a collisionless particle [13]. This is the only treatment, known to us, that accurately describes fast ion orbits and their distribution function in realistic, high-β, non-circular equilibria like those of Ref. 85. However, Mikkelsen and Post can do such calculations in principle. Recently, Kolesnichenko and Yavorskii [113] have modeled 3.5-Mev alpha losses from non-circular tokamaks, but they did not study slowing down effects. In addition, our model treats first-orbit losses, trapping effects and slowing-down drifts. The COM approach does find the distribution function, and since a 3-D (+ time) equation is solved, it is possible to derive scaling laws.

8.2 Guiding-Center Equation

Three constants-of-motion (COM) are required to fully describe the guiding-center motion of a collisionless particle in an axisymmetric tokamak. The usual COM are E (the energy), μ (the magnetic moment), and P_ϕ (the toroidal conanical angular momentum), but this set is inconvenient for our problem. Following Rome and Peng [13], we pick v (the ion speed), ψ_x (the maximum value of the poloidal flux function along the guiding-center orbit, where ψ is increasing from the magnetic axis), and ζ(the cosine of the angle between the parallel component of plasma current and the ion velocity, i.e. $\zeta = \vec{J}_\parallel \cdot \vec{v}/(|\vec{J}_\parallel|v)$ at ψ_x). The remainder of this chapter summarizes the pertinent results of Ref. 13, which will then be applied to the present problem.

First to be considered are the COM in terms of E, μ, and P_ϕ, from which the guiding center motion can be derived. The toroidal canonical angular momentum is conserved through first order in gyroradius [86] when written in terms of guiding-center coordinates. Assuming ideal MHD equilibrium [85], P_ϕ can be written in mks units as:

$$P_\phi = mv\gamma\eta F/B - Ze\psi = mv\gamma\zeta F_x/B_x - Ze\psi_x, \tag{8.1}$$

where m and Ze are the ion mass and charge, $1/\gamma = \sqrt{1-(v/c)^2}$, c = speed of light, $F = F(\psi) = RB_\phi$. Also, η is the cosine of the local pitch angle (i.e. $\eta = \vec{J}_\parallel \cdot \vec{v}/(|\vec{J}_\parallel|v)$ evaluated at ψ), and the subscript "x" in (8.1) denotes evaluation at ψ_x. A cylindrical coordinate system (R,ϕ,z) is used. Quantities obtained from

the MHD equilibrium [85] include: the poloidal flux function, ψ, the magnitude of the magnetic field, B, the function $F(\psi)$, and their derivatives. The magnetic moment can be rewritten in terms of these same variables, yielding:

$$(1-\zeta^2)/B_x = (1-\eta^2)/B. \tag{8.2}$$

Rewriting (8.2), the parallel velocity at any point on the orbit is $v = v\eta = \pm v\sqrt{1-(1-\zeta^2)B/B_x}$, which can be substituted into (8.1) to obtain the orbit equation, $B = B_o(\psi)$:

$$B = B_x / \left\{ \tfrac{1}{2}(1-\zeta^2) + \{ \tfrac{1}{4}(1-\zeta^2)^2 + (F_x/F)^2[\zeta-(G_x c/v\gamma) \times (1-\psi/\psi_x)]^2 \} \right\} \tag{8.3}$$

where the dimensionless constant, $G_x = ZeB_x\psi_x/mcF_x$. Picking the COM coordinates (v,ζ,ψ_x) uniquely defines an orbit, which is parameterized by ψ over the interval $\psi_n \leq \psi \leq \psi_x$. Here, ψ_n is the minimum value of ψ on the orbit.

There is a one-to-one correspondence between the spatial coordinates (R,z) and the (B,ψ) coordinates of the guiding center. Here, the B = constant and ψ = constant surfaces constitute a non-orthogonal system which can be inverted to find (R,z). This is particularly difficult in the equatorial plane (z=0) where the B- and ψ- surfaces are parallel. To establish the allowed domain in B-ψ space for all possible orbits, we first plot (see Fig. 8.1) B

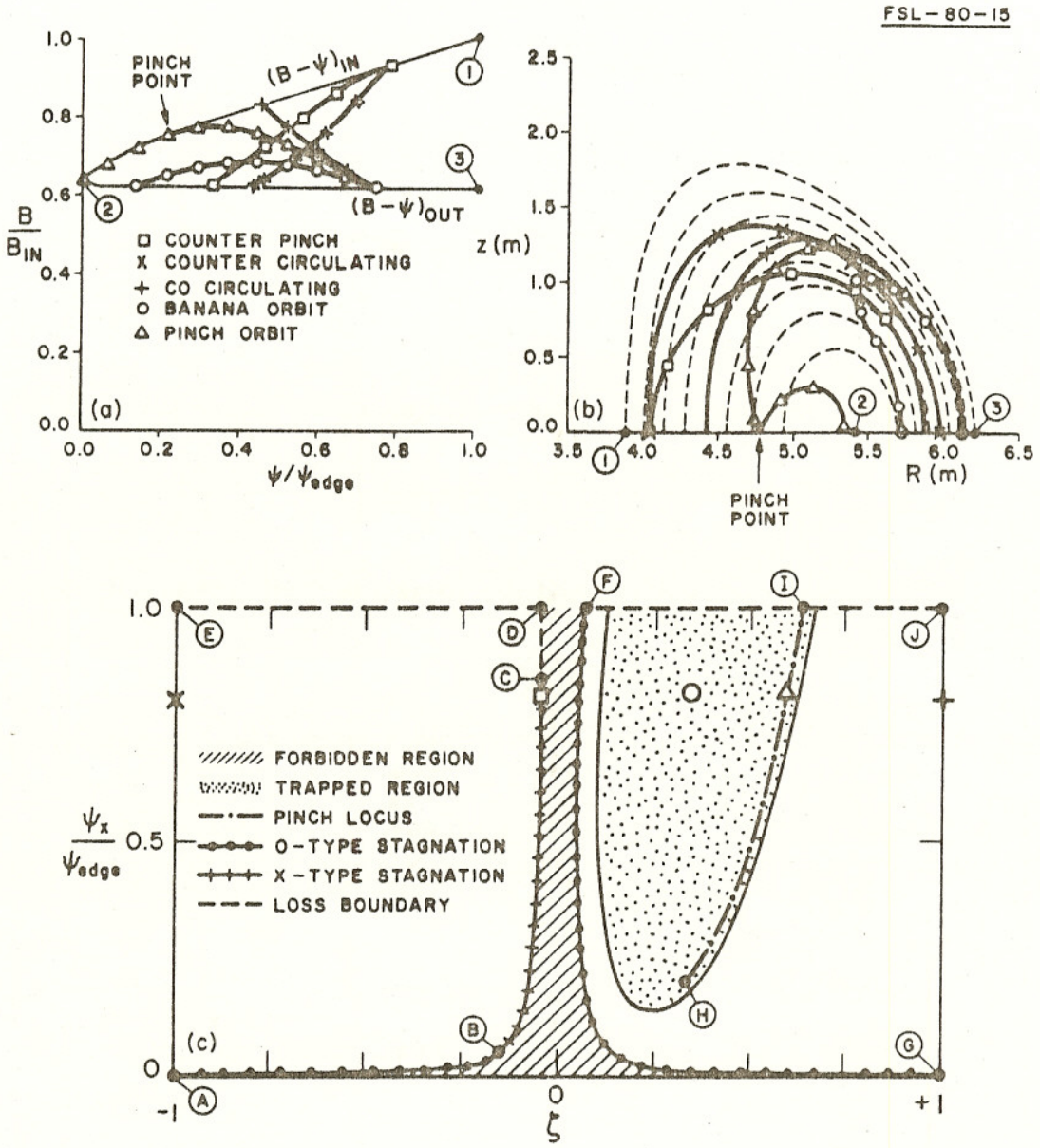

Figure 8.1 The correspondence between orbits in (a) (B,ψ) space and (b) configuration (R,z) space (taken from Ref. 13), with the resulting orbit loci in phase space for v=constant. Up-down symmetry permits only z>0 part of orbits.

along the equatorial plane versus ψ (normalized to the ψ-value at the plasma edge, ψ_{edge}). In Fig. 8.1a, the curve segment between points 1 and 2, labelled $(B\text{-}\psi)_{IN}$, is obtained from Fig. 8.1b by moving (on the equatorial plane) from point 1 (at the inboard edge of the equilibrium) to point 2 (at the magnetic axis). Similarly, in Fig. 8.1a, the curve segment between points 2 and 3, labelled $(B\text{-}\psi)_{OUT}$, is obtained from Fig. 8.1b by moving from point 2 to 3 (at the outboard edge of the plasma). Particle orbits move monotonically in ψ, intersecting the $(B\text{-}\psi)_{EQ}$ curve (composed of $(B\text{-}\psi)_{IN}$ and $(B\text{-}\psi)_{OUT}$) usually only twice: at (B_x,ψ_x) and at (B_n,ψ_n). Several examples of orbit trajectories in B-ψ space are shown in Fig. 8.1a with the corresponding configuration space orbits in Fig. 8.1b[13]. The sequence of co-going orbits (evolving from co-circulating to pinch, trapped, and o-type stagnation) is obtained by decreasing ζ from +1, for a fixed value of ψ_x on the outboard side of the magnetic axis. The corresponding points in ψ_x-ζ phase space (v = constant) are shown in Fig. 8.1c. Similarly, the sequence of counter-going orbits (evolving from counter-circulating to counter x-type stagnation) is obtained by increasing ζ from -1, for a fixed value of ψ_x on the inboard side of the magnetic axis.

The COM-space topology in the v = constant plane, is shown in Fig. 8.1c. The boundaries (loss, stagnation orbit) and regions (forbidden, trapped particle) determine the transport mechanisms for

fast ions. Consequently, the detailed features of the (v,ζ,ψ_x) space are examined next.

8.3 Stagnation Orbit Boundary

The stagnation orbits (the counter x-type and o-type stagnation) occur when the $(B-\psi)$ orbit trajectory is tangent to $(B-\psi)_{EQ}$ at ψ_x:

$$B'_{ex} = B'_{ox} = \frac{2B_x\zeta}{1+\zeta^2}\left(\frac{\zeta F'_x}{F_x} - \frac{G_x c}{v\gamma\psi_x}\right) \tag{8.4}$$

Here, B'_{ex} indicates the ψ-derivative (at ψ_x) of the *equilibrium* field in the equatorial plane; B'_{ox} is the ψ-derivative of the *orbit* equation (8.3) at ψ_x. The o-type stagnation orbit (a 'point' orbit in both $B-\psi$ and R-z space) occurs when the curvature and $\vec{B}\times\nabla B$ drifts exactly cancel the poloidal motion along a field line. In Fig. 8.1c, the boundaries ABCD and FG are given by (8.4). The region between these two boundaries is forbidden; corresponding orbits in $(B-\psi)$ space lie below $(B-\psi)_{OUT}$ or above $(B-\psi)_{IN}$ and thus do not constitute physically realizable trajectories in (R-z) space. Since orbits can also be labeled by v,ψ_n, and $\lambda = (\vec{J}_{\parallel}\cdot\vec{v})/(|\vec{J}_{\parallel}|\ v)$ at ψ_n, the forbidden region also serves to make the labeling unique by grouping all the ambiguous points associated with (v,λ,ψ_n) into the forbidden region.

The second important internal boundary is the locus of pinch orbits (line HI in Fig. 8.1c), occurring when the $(B-\psi)_{orbit}$ trajectory is tangent to $(B-\psi)_{EQ}$ at the pinch point, ψ_p and is given by:

$$\eta_p^4 \{-4B_xB_p^3F_x^2 + B_x^2[(1-\psi_p/\psi_x)(2B_pF_p' - F_pB_p') + 2B_pF_p]^2\}$$

$$+\eta_p^2\{-4(B_p-B_x)B_p^3F_x^2 - 2B_x^2B_p'F_p(\psi_x-\psi_p)[(1-\psi_p/\psi_x)(2B_pF_p'-F_pB_p') + 2B_pF_p]\}$$

$$+ \{B_xB_p'F_p(1-\psi_p/\psi_x)]^2 = 0 \tag{8.5}$$

and

$$\zeta = \sqrt{1-(1-\eta_p^2)B_x/B_p} \tag{8.6}$$

The subscript 'p' indicates evaluation at the pinch point (see Figs. 8.1a-b). As before, primed variables are derivates with respect to ψ. Equation (8.5) is solved by choosing a point (B_x,ψ_x) in the equatorial plane (outboard side), then searching (numerically) through values of (B_p,ψ_p) lying in the equatorial plane (inboard side). The corresponding value of η_p^2 is given by solving the biquadratic equation (8.5), $c_1\eta_p^4 + c_2\eta_p^2 + c_3 = 0$:

$$\eta_p=-\sqrt{-\frac{c_2}{2c_1}\left[1 - \mathrm{sgn}\left(\frac{c_2}{2c_1}\right)\sqrt{1-4c_1c_3/c_2^2}\right]} \tag{8.7}$$

from which ζ is found using (8.6). Note that the minus sign is used

in (8.7) so that $|\eta_p| \leq 1$. The search is successful when the desired value of v/c is obtained from

$$u = \frac{\gamma v}{c} = G_x \eta_p \Bigg/ \left[\frac{\eta_p^2 B_x}{F_x}\left(\frac{F_p'}{B_p} - \frac{F_p B_p'}{B_p^2}\right) - \tfrac{1}{2}\,(1-\zeta^2)\,\frac{F_p B_p'}{F_x B_p} \right] , \tag{8.8}$$

$$\text{with } v/c = u \Big/ \sqrt{1+u^2} \ . \tag{8.9}$$

The end of the pinch boundary (point H in Fig. 8.1c) is found when the inner (counter-going) loop of the x-type stagnation orbit shrinks to a point ($\psi_n \to \psi_p$ at point B in Fig. 8.1c) and occurs when $B''_{ep} = B''_{op}$ in the equatorial plane (inboard side). The resulting condition is a biquadratic in η_p (the cosine of the pitch angle at ψ_p), $c_1' \eta_{pe}^4 + c_2' \eta_{pe}^2 + c_3' = 0$:

$$\begin{aligned} &\eta_{pe}^4 [4F_p''/F_p - 4B_p'F_p'/B_pF_p - 2B_p''/B_p + 3(B_p'/B_p)^2] \\ &+\eta_{pe}^2 [6(B_p'/B_p)^2 - 2B_p''/B_p - 4B_p'F_p'/B_pF_p] - (B_p'/B_p)^2 = 0 \end{aligned} \tag{8.10}$$

which has the solution:

$$\eta_{pe} = - \sqrt{- \frac{c_2'}{2c_1'} \left[1 - \operatorname{sgn}\left(\frac{c_2'}{2c_1'}\right) \sqrt{1 - 4c_1'c_3'/(c_2')^2} \right]} \ . \tag{8.11}$$

As before, the minus sign in (8.11) is required for $|\eta_{pe}| \leq 1$. It is necessary to (numerically) search for the value of ψ_p which produces the desired value of v/c from (8.9) and:

$$u = \frac{\gamma v}{c} = G_p \eta_{pe} / [\eta_{pe}^2 F_p'/F_p - \tfrac{1}{2}(1+\eta_{pe}^2) B_p'/B_p]. \tag{8.12}$$

The corresponding values of ψ_x and ζ are found by searching for the ψ_x crossing via the orbit equation:

$$B = B_p \Bigg/ \left\{ \frac{1-\eta_p^2}{2} + \left\{ \left(\frac{1-\eta_p^2}{2} \right)^2 + \left(\frac{F_p}{F} \right)^2 \left[\eta_p - \frac{G_p c}{v\gamma} \left(1 - \frac{\psi}{\psi_p} \right) \right]^2 \right\}^{\frac{1}{2}} \right\} , \tag{8.13}$$

where $G_p = ZeB_p\psi_p/mcF_p$.

8.4 Connectivity of Orbit Topology

The next important feature of the orbit topology is the connectivity of the two halves of phase space via scattering across the pinch orbit. Figure 8.2 illustrates the ways that scattering occurs among orbits adjacent to the pinch orbit. The arrows, labelled 1 in Figs. 8.2a-b, correspond to scattering from a counter x-type stagnation orbit (...), across the pinch orbit (—), to a fattest-banana (—•—). The arrows, labelled 2, denote scattering from a fattest banana (—•—), across the pinch orbit to either a counter x-type stagnation (...) or to an outermost kidney (— —) orbit. Finally, the arrows, labelled 3, indicate scattering from an outermost kidney orbit (— —), across the pinch orbit (——), to a fattest banana (—•—). It will be necessary to account for all these processes, in the solution for alpha slowing down, by conserving the resultant velocity-space particle fluxes.

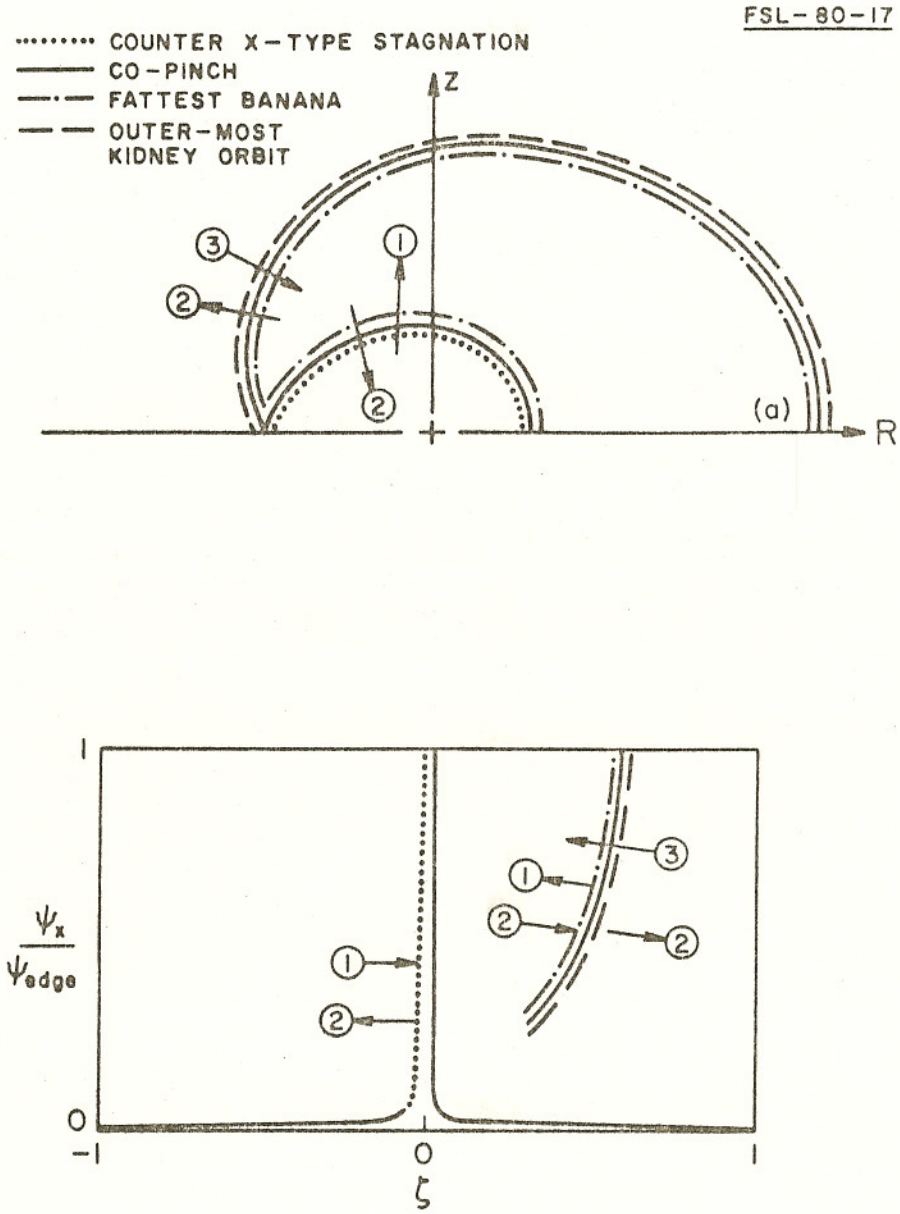

Figure 8.2 The pinch orbit in (R,z) space, together with neighboring orbits is shown in (a). The corresponding directions of the particle fluxes in (ψ_x, ζ) space is depicted in (b) for v=constant.

8.5 Loss Boundaries

The last important feature is the loss boundary (lines CDE and FIJ in Fig. 8.1c). Losses occur when an orbit intersects the wall at ψ_W, yielding $\psi_X \geq \psi_W$ as the condition for the boundaries DE and FIJ in Fig. 8.1c. Particles which drift or scatter across the boundary CD, in Fig. 8.1c, are also lost to the wall. This corresponds to an orbit evolving from counter-circulating, to counter x-type stagnation (the inner loop of a pinch), to banana (arrow 1 in Fig. 8.2). It is the trapped orbit (fattest banana), which has $\psi_X > \psi_W$ and causes the particle to be lost to the wall.